



# A “trapezoidal” relationship between solar radiation and chlorophyll concentrations at the center of the South Pacific Gyre

Dongmei Lian<sup>a</sup>, Xin Liu<sup>a,\*</sup>, Edward A. Laws<sup>b</sup>, Tongtong Liu<sup>a</sup>, Jingxiao Wang<sup>a</sup>, Shaoling Shang<sup>a</sup>, Zhongping Lee<sup>a,\*</sup>

<sup>a</sup> State Key Laboratory of Marine Environmental Science, Xiamen University, Xiamen, Fujian 361102, China

<sup>b</sup> Department of Environmental Sciences, College of the Coast & Environment, Louisiana State University, Baton Rouge, LA 70803, USA

## ARTICLE INFO

### Keywords:

Phytoplankton  
Photoacclimation  
Nutrients  
Grazing pressures  
Steady and non-steady state

## ABSTRACT

Understanding the driving mechanism of phytoplankton dynamics is key to forecasting future changes in the ocean. Here, we report an apparent “trapezoidal” relationship between chlorophyll concentrations (Chl) and surface photosynthetically available radiation (PAR(0)) at the center of the South Pacific Gyre (cSPG) based on 18 years of MODIS Aqua measurements. A comparison of Chl with a photoacclimation model revealed that photoacclimation alone could not explain the temporal dynamics of Chl. Instead, the Chl dynamics were explained by a combination of photoacclimation, nutrient limitation, and the grazing pressure of zooplankton at different times throughout the year. An annual “trapezoidal” spiral relationship between Chl and PAR(0) suggested that the steady state of phytoplankton populations at the cSPG could be influenced by the alternation of co-regulation mechanisms during a year. Because this same pattern occurs in other subtropical gyres, this understanding of the underlying mechanisms not only facilitates simulating and forecasting phytoplankton dynamics but also provides a new perspective on how multiple stressors may impact phytoplankton communities in a warmer climate.

## 1. Introduction

The abundance of phytoplankton (commonly quantified in terms of chlorophyll concentration, Chl) and their physiological characteristics are strongly affected by a variety of factors (e.g., light, mixing, and grazing pressure from zooplankton) (Behrenfeld et al., 2016; Boyce et al., 2017; McClain, 2009). Previous studies of phytoplankton dynamics have focused on statistical relationships between Chl and the physicochemical and biological characteristics of large- and meso- scale water masses (Cara et al., 2005; Dandonneau et al., 2003; Doney et al., 2003; Dufois et al., 2016; Signorini et al., 2015). These earlier studies have primarily been based on the assumption of steady state (Laws et al., 2000; Plattner, 2005). However, Beninca et al. (2008) have reported the importance of non-steady state dynamics in marine ecology. Though these terms have been used in the context of culture systems, they are still broad concepts in ecology (Harris, 1988; Pahl-Wostl, 1995). In general, a “steady state” reflects complex relationships between various controlling factors and phytoplankton, resulting in steady growth balanced by their removal so that the phytoplankton community

remains constant over time (Rojo & Álvarez-Cobelas, 2003). A “non-steady state” condition, in contrast, refers to a dynamic scenario where multiple nested and interacting processes undergo alternating changes that lead to fluctuations of the phytoplankton community over time (Beninca et al., 2008; Naselli-Flores et al., 2003). The different characteristics of steady state and non-steady state dynamics lead to uncertainty in the mechanisms that drive phytoplankton dynamics, and that uncertainty confounds predictions of future trends.

Previous ocean studies based on the non-steady state assumption have mostly focused on the destabilized ecosystems, which included large perturbations that, such as blooms or typhoons (Boss & Behrenfeld, 2010; Xiu & Chai, 2021). These have been mostly short-term, event-based process studies with prominent spatiotemporal heterogeneity. Because of the complexity of water-mass interactions in the ocean, there have been few studies based on the non-steady state assumption in oligotrophic waters. Studying the steady state and non-steady state dynamics of phytoplankton requires documenting temporal dynamics in a particular water mass over a long time (Wu & Loucks, 1995). Such a water mass should be seldom perturbed by interactions with external

\* Corresponding authors.

E-mail addresses: [liuxin1983@xmu.edu.cn](mailto:liuxin1983@xmu.edu.cn) (X. Liu), [zpli2015@xmu.edu.cn](mailto:zpli2015@xmu.edu.cn) (Z. Lee).

<https://doi.org/10.1016/j.pocean.2024.103281>

Received 23 November 2023; Received in revised form 13 April 2024; Accepted 13 May 2024

Available online 16 May 2024

0079-6611/© 2024 Elsevier Ltd. All rights are reserved, including those for text and data mining, AI training, and similar technologies.

water masses, and the research methodology should involve observing the phytoplankton dynamics over a long period. To meet this requirement, we focused on the surface layer at the center of the South Pacific Gyre (cSPG) (see Fig. 1a), which is a mode water and is nearly vertically homogeneous in the upper water column (Talley, 1999). It is influenced very little by interactions with external water masses and allochthonous inputs (McClain et al., 2004; Middleton & Kang, 2017; Zehr & Capone, 2020; Zhang et al., 2015). The waters of the cSPG are very clear (Claustre et al., 2008), and the phytoplankton Chl dynamics has been assumed driven by photoacclimation (Behrenfeld et al., 2016) without the influence of external factors, such as land runoff or cultural eutrophication. Because of the remoteness of this unique water mass, we made observations via satellite remote sensing to meet the requirements for long-term consistency in our study of Chl dynamics in the cSPG.

We therefore used data from satellite ocean color remote sensing along with a photoacclimation model to evaluate the underlying mechanisms that drive phytoplankton Chl dynamics in the cSPG. We hypothesized that the seasonal variation of Chl in the cSPG was a dynamic steady state regulated not solely by photoacclimation but rather a complex process. We found that co-regulation by different processes drove Chl dynamics during different periods of the year in the cSPG. Moreover, a long-term “trapezoidal” relationship between Chl and PAR(0) implied that phytoplankton may be influenced by the alternation of co-regulation mechanisms throughout the year. Further, we extended the analyses to other subtropical gyres and observed the same causative mechanisms. The results of this study help to explain the temporal dynamics of phytoplankton in such water masses.

## 2. Data and methods

### 2.1. Data source

Standard Level 3 products of Chl, PAR(0), diffuse attenuation coef-

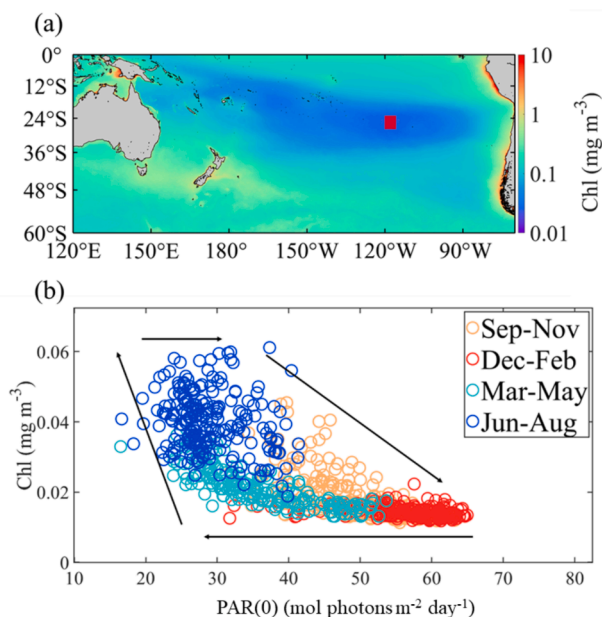


**Fig. 1.** (a) The red square is designated as cSPG (23° - 28° S and 115° - 120° W). The background color is the average climatological Chl derived from MODIS Aqua, which was downloaded from NASA OBPG. (b) The “trapezoidal” relationship between Chl and PAR(0) at cSPG, where both products were downloaded from NASA OBPG. They have a spatial resolution of 9 km and a temporal resolution of 8-day from 2002 to 2020. Colors are denoted by seasons. Orange circles: austral spring (September to November); Red circles: austral summer (December to February); Green circles: austral autumn (March to May); Blue circles: austral winter (June to August).

ficient at 490 nm ( $K_d(490)$ ), particle backscattering coefficient at 443 nm ( $b_{bp}(443)$ ), and sea-surface temperature (SST) for the area bounded by 23–28° S and 115–120° W (see the red box in Fig. 1a) derived from the MODerate resolution Imaging Spectroradiometer on the Aqua satellite (MODIS Aqua) were downloaded from the National Aeronautics and Space Administration (NASA) Ocean Biology Processing Group. The area includes the most oligotrophic waters of the global ocean (26° S, 115° W) (Claustre et al., 2008). Whereas different algorithms have been used to generate the aforementioned satellite products, for consistency with the photoacclimation model developed by Behrenfeld et al. (2016), Chl was derived with the Ocean Color Index (OCI) algorithm (Hu et al., 2012),  $b_{bp}(443)$  by the Garver-Siegel-Maritorena algorithm ( $b_{bp443}^{GSM}$ ) (Maritorena et al., 2002), and  $K_d(490)$  by the 490–547 band ratio algorithm (Austin & Petzold, 1981; Werdell & Bailey, 2005). Following Morel et al. (2007) and Behrenfeld et al. (2016), the diffuse attenuation coefficient for PAR ( $K_{PAR}$ ) was calculated from  $K_d(490)$ , and  $C_{ph}$  (phytoplankton carbon) was estimated based on  $b_{bp443}^{GSM}$  as in Behrenfeld et al. (2005) and Westberry et al. (2008). The spatial resolution of these data is 9 km, with a temporal resolution of 8 days for the period from July 2002 to December 2020. Daylength (in hours) was calculated as a function of date and latitude following Kirk (1983) and was used to convert the daily PAR(0) product to hourly PAR(0) ( $\text{mol photons m}^{-2} \text{h}^{-1}$ ) by dividing by daylength. The MLD data were obtained from the HYbrid Coordinate Ocean Model (HYCOM) with the same spatial and temporal resolutions for the same period.

### 2.2. Zooplankton data

Total zooplankton biomass data were obtained from the Coastal and Oceanic Plankton Ecology, Production, and Observation Database (COPEPOD). Because there were no data collected in the cSPG, data from the nearest area (10–30° S and 90–180° W) in the SPG region were selected to represent observations in the targeted area. These data on total zooplankton biomass were collected using nets with varying mesh sizes ( $\mu\text{m}$ ). Due to the phytoplankton community of cSPG is dominated by pico-sized phytoplankton, the mesozooplankton and higher-level zooplankton would only have few influences on it. Thus, the data which was identified as “fish (unidentified eggs or larvae)” were excluded from the analysis. The remaining data (Number (N) = 357) were standardized to common units of zooplankton carbon biomass, which included two different units: ‘Zooplankton wet weight’ ( $\text{mg m}^{-2}$ ), ‘Zooplankton displacement volume’ ( $\text{mL m}^{-2}$ ), and ‘Zooplankton settled volume’ ( $\text{mL m}^{-2}$ ). Meanwhile, these data included each month from spring to autumn, but there were no data for June and July during the austral winter.

### 2.3. Photoacclimation model

The photoacclimation model used in this study followed that of Behrenfeld et al. (2016), which provides a steady-state equation for the ratio ( $\theta$ ) of phytoplankton carbon to chlorophyll concentration, with  $\theta$  modeled as a function of light in the mixed layer (Eqs. 1–5). The input parameters of this photoacclimation model include hourly PAR(0),  $K_{PAR}$ , and MLD, with a math function as (Behrenfeld et al., (2016)):

$$\theta = \theta_{DM} \Delta \theta_{SM} \quad (1)$$

with  $\theta_{DM}$  for photoacclimation under deep-mixing scenarios when the mixed-layer depth is deeper than the euphotic zone depth ( $Z_{eu}$ ) (Eq. (2)). The variable  $\Delta \theta_{SM}$  is a term introduced to correct for a shallow mixed layer (MLD <  $Z_{eu}$ ) (Behrenfeld et al., 2016) and is expressed using Eqs. (3–4),

$$\theta_{DM} = c_1 e^{c_2 \frac{PAR(0)^{0.45}}{K_{PAR}}} \quad (2)$$

Here  $c_1 = 19 \text{ g C (g Chl)}^{-1}$  and  $c_2 = 0.038 \text{ m}^{-1} (\text{mol photons m}^{-2})$

$h^{-1})^{-0.45}$  as model constants. The term  $\Delta\theta_{SM}$  is.

$$\Delta\theta_{SM} = \begin{cases} \frac{1 + e^{-0.15 PAR(0)}}{1 + e^{-3 I_{ML}}}, & MLD < \frac{6}{K_{PAR}} \quad (3) \end{cases}$$

$$1, \quad MLD \geq \frac{6}{K_{PAR}} \quad (4)$$

with  $I_{ML}$  is the irradiance at half of the mixed layer depth and was calculated following Westberry et al. (2008):

$$I_{ML} = PAR(0)e^{-0.5 K_{PAR} MLD} \quad (5)$$

Once  $C_{ph}$  and  $\theta$  have been determined, the concentration of phytoplankton chlorophyll based on phytoplankton carbon and photoacclimation –  $Chl(\theta)$  – can be calculated from Eq. (6):

$$Chl(\theta) = \frac{C_{ph}}{\theta} \quad (6)$$

If the data and photoacclimation model are consistent with each other, the modeled  $Chl(\theta)$  and observed  $Chl$  will equal to each other. In this case, photoacclimation dominates  $Chl$  dynamics. If  $Chl(\theta)$  does not equal to  $Chl$ , mechanisms other than photoacclimation will affect cellular  $Chl$  levels (Behrenfeld et al., 2016). Based on Behrenfeld et al. (2016), the uncertainty is estimated to be  $\sim 20\%$  for  $\theta$  in SPG. Meanwhile, Hu et al. (2012) have reported that there is  $\sim 10\%$  uncertainty of  $Chl$  when using Ocean Color Index (OCI) algorithm. We thus set a  $\sim 30\%$  uncertainty when comparing satellite  $Chl$  with  $Chl(\theta)$ . Note that, at spatially averaged and monthly scales, the uncertainties are much less than  $30\%$  (Qi et al., 2017). While acknowledging the potential influence of non-algal matter or taxonomy on the conversion from  $b_{bp}$  to  $C_{ph}$  (Fox et al., 2022; Karl et al., 2022), it is noteworthy that the conversion remains relatively consistent in oligotrophic southern hemisphere (including cSPG) throughout the year (Serra-Pompei et al., 2023). Additionally, the coefficients of variation (CV) of  $\theta$  ( $\sim 0.61$ ) was 3.6 times the CV of  $C_{ph}$  ( $\sim 0.17$ ), which indicated that  $\theta$  has much more influence on the modeling of  $Chl(\theta)$  than  $C_{ph}$ . Thus, we assumed that the uncertainty associated with  $C_{ph}$  is encompassed within the above mentioned  $30\%$ .

#### 2.4. Statistical analyses

A one-sample  $t$ -test was used to test for differences between two datasets (e.g., zooplankton biomass during two periods of time). Whether the mean of a dataset was consistent with a hypothetical value was determined on the basis of the  $t$  statistic and the corresponding type I error rate (Gerald, 2018). The  $p$ -value ( $p$ ) and  $t$ -value ( $t$ ) were used to assess statistical significance. One-sample  $t$ -tests were carried out in OriginPro Version 2022 (OriginLab Corporation, Northampton, MA, USA). To characterize the influence of environmental factors (MLD,  $\exp(-3I_{ML})$  and SST) on  $Chl$ , the multiple linear regression (MLR) analyses were carried out to describe the relationships between all three factors and  $Chl$  (Cohen et al., 2013). The MLR is a statistical method for predicting the result of a dependent variable by using a number of explanatory independent variables. The statistical parameter (e.g., coefficient of determination ( $R^2$ ),  $p$ ) could represent the influences of independent variables on dependent variable. MLR were conducted using the “regress” function of MATLAB Version 2019a to characterize how environmental factors (MLD,  $\exp(-3I_{ML})$  and SST) affect the  $Chl$  (The MathWorks, Inc., Natick, Massachusetts, United States). Due to the relationships between MLD and nutrients (Wilson & Coles, 2005),  $\exp(-3I_{ML})$  and photoacclimation (Behrenfeld et al., 2005; Behrenfeld et al., 2016), SST and grazing pressure of zooplankton (O’Brien et al., 2013), we used MLD,  $\exp(-3I_{ML})$  and SST as the indicator of nutrients, photoacclimation and grazing pressures by zooplankton, respectively.

#### 2.5. Data availability

Satellite data are available at: <https://oceancolor.gsfc.nasa.gov/>, and zooplankton data are available at: <https://www.st.nmfs.noaa.gov/copepod/about/databases.html>.

### 3. Results and discussion

#### 3.1. A trapezoidal pattern between $Chl$ and $PAR(0)$ in the cSPG

For the first time, we found that there is an apparent trapezoidal pattern (see Fig. 1b) between  $Chl$  and  $PAR(0)$  based on an almost 18 years of measurements by the MODIS Aqua over the cSPG water. The  $Chl$  demonstrates distinct seasonal variations in the ultra-oligotrophic ocean (i.e. cSPG), indicating high variable  $Chl$  even under the same light intensity. Specially, we found that  $Chl$  decreased in austral spring (right non-parallel side), remained almost constant in austral summer (bottom side), and then rapidly increased in austral autumn and winter (left non-parallel side). Meanwhile, the range of  $Chl$  during June (from  $\sim 0.03$  to  $0.05 \text{ mg m}^{-3}$ ) is similar to the range in July (from  $\sim 0.03$  to  $0.06 \text{ mg m}^{-3}$ ) (upper side). Moreover, the magnitude of the  $Chl$ -decline rate with increasing  $PAR(0)$  (from 35 to  $50 \text{ mol photons m}^{-2} \text{ day}^{-1}$ ) is much less than the  $Chl$ -increase rate with a decreasing  $PAR(0)$  (from 35 to  $25 \text{ mol photons m}^{-2} \text{ day}^{-1}$ ). This trapezoidal pattern revealed large fluctuations of  $Chl$  at similar  $PAR(0)$ . For example,  $Chl$  varied by a factor of  $\sim 3$  for  $PAR(0)$  of  $\sim 35 \text{ mol photons m}^{-2} \text{ day}^{-1}$ . Recent studies have suggested that photoacclimation is the dominant process responsible for the temporal variations of  $Chl$  in the SPG (Behrenfeld et al., 2016). We therefore tried to analyze the role photoacclimation and other processes played in this trapezoidal pattern.

#### 3.2. Periods when photoacclimation dominates

To understand the importance of photoacclimation on  $Chl$  dynamics in the cSPG, we compared the  $Chl$  estimated from a photoacclimation model ( $Chl(\theta)$ ) with  $Chl$  obtained from ocean color remote sensing for each month of the year (see Fig. 2). Whereas  $Chl$  was in the range  $0.01\text{--}0.06 \text{ mg m}^{-3}$ ,  $Chl(\theta)$  was in the range  $0.005\text{--}0.1 \text{ mg m}^{-3}$ .  $Chl(\theta)$  was significantly (about 1.6 times) higher than  $Chl$  for the months of June to August (southern winter) (one-sample  $t$ -test,  $N = 850$ ,  $p$ -value ( $p$ )  $< 0.01$ , Fig. 2a). The fact that  $Chl(\theta)$  was  $\sim 38\%$  higher on average than  $Chl$  suggested that  $Chl(\theta)$  was overestimated during many months of the year. To determine when photoacclimation was the dominant factor, we plotted the average monthly variation of  $Chl(\theta)/Chl$ , which ranged from  $\sim 1.0$  to  $1.7$ . During the months of January-March and September-October, the ratio of  $Chl(\theta)/Chl$  ranged from  $\sim 1.0$  to  $1.2$ . Considering the uncertainties associated with the ocean color products from satellites, the implication of these values is that photoacclimation provided a plausible explanation for the  $Chl$  dynamics during these months. However, the fact that the monthly averages of  $Chl(\theta)/Chl$  for the other months were in the range  $\sim 1.4$  to  $1.7$  suggested that photoacclimation alone might not have been the only process driving  $Chl$  variations during these months. Other processes or mechanisms also played important roles in the dynamics of  $Chl$  during these periods.

#### 3.3. The roles of nutrients and zooplankton grazing during the period April to August

$Chl(\theta)$  were much higher than  $Chl$  from April to August. During this period, the  $I_{ML}$  decreased sharply from  $\sim 2.5$  to  $0.5 \text{ mol photons m}^{-2} \text{ h}^{-1}$  while the MLD deepened ( $\sim 56.2\text{--}120.8 \text{ m}$ ), and  $I_{ML}$  fluctuated around  $0.5 \text{ mol photons m}^{-2}$  when the MLD exceeded  $\sim 100 \text{ m}$  (see Fig. 3). The deep MLD suggested that while nutrients were brought up from the nutricline into the mixed layer, there was also enhancement of a darkening, cooling, and dilution effect during this period (Behrenfeld, 2010; Boss & Behrenfeld, 2010). Above all, when the MLD is shallow, the  $I_{ML}$  is

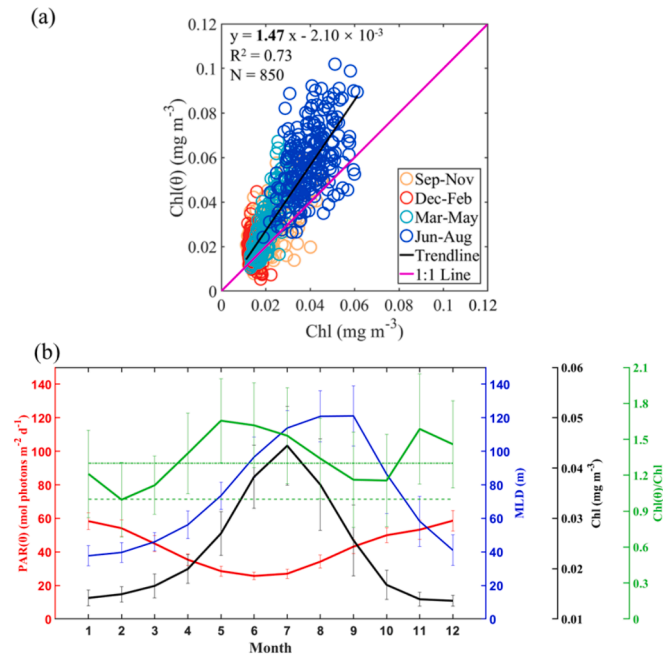


**Fig. 2.** (a) Relationship between Chl(θ) and Chl. The color of the points represents seasonal periods, consistent with Fig. 1b. The black line is a linear fit. (b) Monthly variation of PAR(0) (red line), mixed-layer depth (MLD, blue line), Chl (black line) and Chl(θ)/Chl (green line) at cSPG. The green dashed line represents the value of 1, and the green dotted line indicates the value of 1.3, which is the line of acceptable error range.

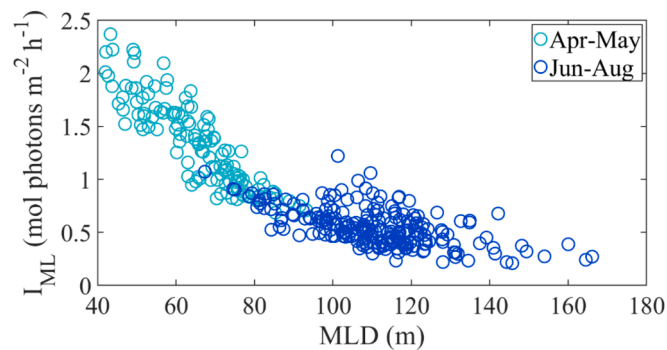


**Fig. 3.** A relationship between MLD and I<sub>ML</sub> (N = 349) from April to August at cSPG.

higher, indicating that during this time, phytoplankton encounter more nutrient limitation than light limitation. Conversely, when the MLD is deep and the I<sub>ML</sub> is lower, the phytoplankton is under stronger light limitation compared to nutrient limitation. Overall, the results suggested that there was a transition from nutrient limitation to light limitation from April to August.

Chl was found increased from April to July (~0.02 – 0.04 mg m<sup>-3</sup>), but decreased in August (~0.03 mg m<sup>-3</sup>). During April to July, the increased supply of nutrients would have enhanced the growth rate of phytoplankton during the MLD-deepening process. Meanwhile, during the period of MLD deepening, the loss rates of phytoplankton might have been reduced based on the decreased encounter rates with zooplankton through “dilution effect” (Boss & Behrenfeld, 2010). This may have further promoted phytoplankton growth rates. Moreover, within the time of decreasing I<sub>ML</sub> and temperature, lower light and temperature might also have diminished the digestion rates of zooplankton (Moeller et al., 2019), potentially also resulting in lower grazing pressures on phytoplankton during this period. Thus, the loss rates of phytoplankton

would have been reduced as a result of the lower light, lower temperature, and decreased encounter rates with zooplankton during the period of MLD deepening (Behrenfeld, 2010; Boss & Behrenfeld, 2010; Landry & Hassett, 1982; Landry et al., 1995).

The scenario shifts in August, while during August, the MLD increased further to about 120 m (Fig. 2b). Though the nutrients were continuously injected, the much lower I<sub>ML</sub> and temperature was not beneficial to support the phytoplankton growth. Meanwhile, the dilution effect would have been weakened due to the deepening rate of MLD being slower than that from April to July (Fig. 2b), while the recoupling between phytoplankton and zooplankton was becoming to recovered (Boss & Behrenfeld, 2010), potentially explaining the initial increase and subsequent decrease in Chl levels (Fig. 2b). Therefore, in addition to photoacclimation, the variations of nutrients and zooplankton could also have an important influence on the carbon to chlorophyll ratio (θ).

The photoacclimation model separated the whole year of cSPG into three distinct periods: April–August, September–October and January–March, November to December, as demonstrated in Fig. 2b. Thus, we utilized these intervals to construct histograms for θ and C<sub>ph</sub>, which are displayed in Fig. 4. The fact that the satellite-derived θ value for the April–August period was the lowest (the average was ~ 377 g C (g Chl)<sup>-1</sup>) compared with other months of the year (the average was ~ 897 g C (g Chl)<sup>-1</sup>) indicated a comprehensive regulation of the physiological state of phytoplankton by low light and low temperature under nutrient-replete conditions (see Fig. 4a). In addition, compared to other months (C<sub>ph</sub> ~ 12.9 mg m<sup>-3</sup> from September to March), C<sub>ph</sub> during April to August remained at relatively low levels (averaging around ~ 10.6 mg m<sup>-3</sup>) (see Fig. 4b). The indication of these distributions is that a combination of effects resulted in not only a change of physiological state but also a decrease in phytoplankton biomass.

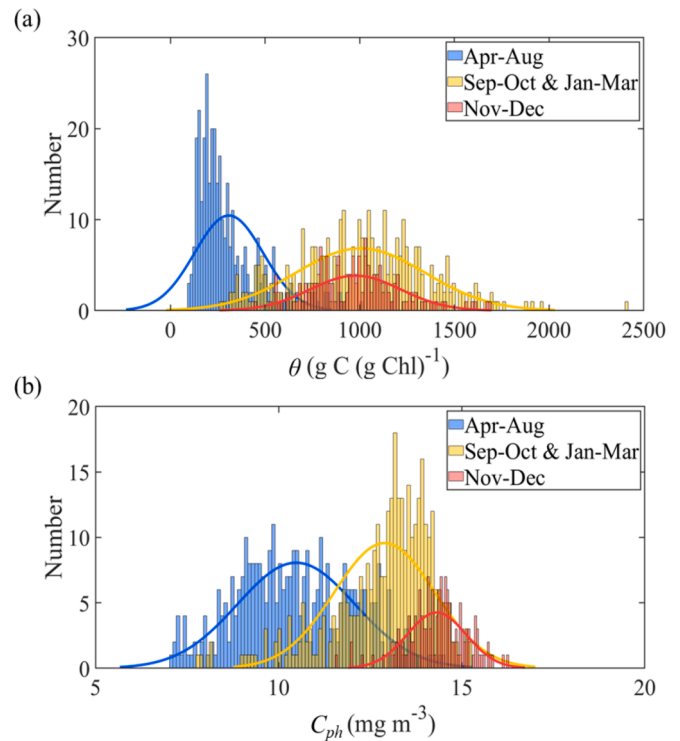


**Fig. 4.** The histograms of average θ from photoacclimation model (a) and C<sub>ph</sub> (b) for April to August (blue), September to October and January to March (yellow), and November to December (red).

### 3.4. The impact of photosynthesis, remineralization, and zooplankton grazing during November–December

The fact that the range of  $\theta$  from November to December was similar to that from September to October and January to March (Fig. 4a) suggested that the effects of photoacclimation on Chl were similar during these periods. However, the relatively high  $C_{ph}$  from November to December ( $\sim 14.3 \text{ mg m}^{-3}$ ) compared to other months ( $\sim 11.7 \text{ mg m}^{-3}$ ) led to higher Chl( $\theta$ ) than Chl for the months of November and December (see Fig. 2b & Fig. 4b).

During November–December, PAR(0) rose to its maximum value ( $\sim 58.6 \text{ mol photons m}^{-2} \text{ day}^{-1}$ ), and the MLD shoaled from  $\sim 58.2$  to  $41.0 \text{ m}$  (see Fig. 2b). During this period, the high PAR and temperature may have enhanced phytoplankton photosynthesis and the digestion rates of zooplankton (Moeller et al., 2019). Meanwhile, the shoaling of the mixed layer could have resulted in not only a decrease of nutrient inputs but also more frequent encounters with zooplankton and hence higher loss rates of phytoplankton (Boss & Behrenfeld, 2010). Increased remineralization due to enhanced grazing and excretion by zooplankton during this shallow-MLD time (Lynam et al., 2017) could have promoted phytoplankton growth. Although higher grazing pressure by zooplankton could have reduced  $C_{ph}$ , the higher rates of phytoplankton photosynthesis and the increased remineralization promoted by higher food-web efficiency would have increased  $C_{ph}$ . The result would have been a relatively constant  $C_{ph}$  maintained at a high level throughout the year. It's worthwhile to note that although some of the phytoplankton consumed by zooplankton may be quickly remineralized and then reabsorbed by phytoplankton, there are changes in their composition, selective grazing, mineralization and assimilation rates, delays effects, and all these variations at different temporal and spatial scales may also contribute to changes in phytoplankton community (Edwards et al., 2012; Geider & La Roche, 2002; Thingstad & Rassoulzadegan, 1995). Therefore, overall, the system was turning over faster during this time. This result suggests that in addition to photoacclimation, high grazing pressures by zooplankton was a key process that regulated Chl dynamics during this period.

Fig. 5 shows that the COPEPOD contained 357 values of zooplankton biomass in the SPG region from September to March. The hypothesized higher grazing pressure during November–December period was consistent with the zooplankton data: As for the comparison of

zooplankton wet weight, the zooplankton biomass ( $\sim 8407.9 \text{ mg m}^{-2}$ ,  $N = 31$ ) was higher in November–December than the zooplankton biomass ( $\sim 6074.8 \text{ mg m}^{-2}$ ,  $N = 6$ ) in the photoacclimation-dominated period (i.e., September to October and January to March); Regarding the comparison of zooplankton settled volume and zooplankton displacement volume, the zooplankton biomass ( $\sim 11.9 \text{ mL m}^{-2}$ ,  $N = 34$ ) also was higher during the period of November–December than the zooplankton biomass ( $\sim 7.6 \text{ mL m}^{-2}$ ,  $N = 286$ ) from September to October and January to March. Both results supported our hypothesis. However, these values do not show significant differences, this may be attributed to the low sample size.

The differences of zooplankton biomass during these two periods could be attributed to a time lag between the peaks of phytoplankton and zooplankton (Almén & Tamelander, 2020; Landry et al., 1997; Sommer, 1988). From September to October, there was a recoupling between phytoplankton and zooplankton in August, but the zooplankton required some time to catch up with the growth of the phytoplankton. From January to March, after most phytoplankton had been consumed, the zooplankton also decreased. From November to December, the close recoupling between plankton increased the turnover rate of the food web, and zooplankton growth was enhanced. The result was higher zooplankton biomass than during the aforementioned periods. In addition to time lag, the complex and multifaceted interaction between phytoplankton and zooplankton, involves intricate trophic relationships and multiple steps within the microbial food web, nutrient cycling and energy transfer might also contributed to the biomass distinctions. It is noteworthy that the phytoplankton community is predominantly dominated by pico-sized phytoplankton in SPG. While within our analysis, the total zooplankton biomass may incorporate meso-zooplankton, which were exerting limited direct effects on the phytoplankton community, indicated this might introduce some error into our analysis. However, the seasonal variation of zooplankton in our study was consistent with the temporal pattern of zooplankton from the ICES reported by the Working Group on Zooplankton Ecology (WGZE) (O'Brien et al., 2013), thus still lending support to our results when considering the error.

Although rapid photosynthesis and remineralization would have increased Chl, photoacclimation and grazing by zooplankton would have decreased Chl. Thus, the complex interactions among photosynthesis, remineralization, photoacclimation, and grazing pressures appeared to have led to a temporarily balanced system. The result is that Chl is nearly constant during this period (see Fig. 1b).

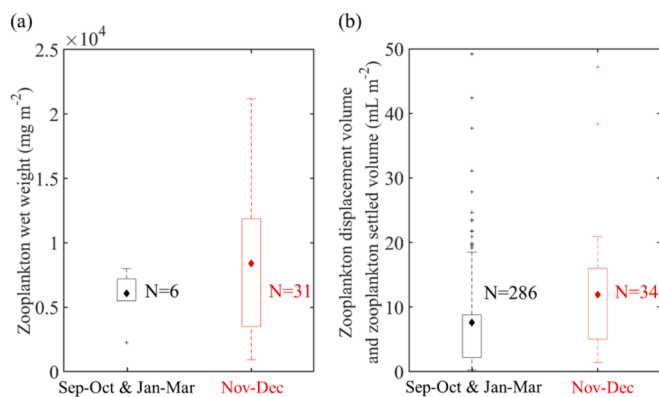


Fig. 5. The zooplankton biomass comparison in two periods. These box plots illustrate the biomass of zooplankton during two periods (Sep-Oct & Jan-Mar, and Nov-Dec), measured in two units: 'Zooplankton wet weight' ( $\text{mg m}^{-2}$ ) (left), and 'Zooplankton displacement volume' and 'Zooplankton settled volume' ( $\text{mL m}^{-2}$ ) (right). The boxes represent the interquartile range (IQR), including the 50 % of data between the first quartile (Q1) and the third quartile (Q3). Whiskers extend to the furthest points within 1.5 times the IQR from the quartiles, excluding outliers. Outliers are marked by plus signs (+) and indicate values beyond 1.5 times the IQR from the nearest quartile. The diamonds represent the mean biomass value of data from each period.

### 3.5. Contrast of the two periods of photoacclimation domination

We observed that although photoacclimation dominated Chl dynamics for the periods of January–March and September–October (Fig. 2b), the change of Chl from September to October ( $\sim 0.03 \text{ mg m}^{-3}$ ) was  $\sim 2.4$  times larger than that from January to March ( $\sim 0.01 \text{ mg m}^{-3}$ ) (Fig. 1b). These results differed from observations that have been reported in the literature: the rate of change of Chl in the subarctic Atlantic is slower when the light is increasing than when it is decreasing, and the rates of change of Chl are similar in the mid-latitude northwest Pacific during the periods of increasing and decreasing light (Graff & Behrenfeld, 2018; Xing et al., 2021). The implication is that the different characteristics of photoacclimation in response to changes of light intensity might be affected by the different physiological conditions of phytoplankton in different marine systems. We thus hypothesized that the physiological status of phytoplankton might differ between September–October and January–March in the cSPG.

Such physiological differences might result in different rates of photoacclimation and would be apparent in the relationship between  $I_{ML}$  and  $\text{Chl}/C_{ph}$  ratio, which was expressed as  $\text{Chl}/C_{ph} = \tau_{\min} + (\tau_{\max} - \tau_{\min}) \exp(-3I_{ML})$  (Behrenfeld et al., 2005; Behrenfeld et al., 2002). Though the  $\text{Chl}/C_{ph}$  ratio of phytoplankton depends on irradiance (Geider, 1987; Macintyre et al., 2002), the minimum of the  $\text{Chl}/C_{ph}$  ratio

( $\tau_{\min}$ ) would decrease with increasing nutrient stress (Laws & Bannister, 1980; Sakshaug et al., 1989), whereas the low-light maximum of the  $\text{Chl}/C_{ph}$  ratio ( $\tau_{\max}$ ) would increase with increasing temperature (Cloern et al., 1995; Geider, 1987). Thus, unlike the photoacclimation model that focused exclusively on light (Behrenfeld et al., 2016) (see Eqs. 1–5 in the photoacclimation section), the  $\tau_{\min}$  and  $\tau_{\max}$  values in this relationship represent the effects of nutrient stress and temperature limitation on photoacclimation, respectively (Behrenfeld et al., 2005; Behrenfeld et al., 2002).

In the case of nutrient stress, the value of  $\tau_{\min}$  that resulted in the best fit for January to March was  $1.1 \times 10^{-3} \text{ mg Chl (mg C)}^{-1}$  ( $N = 214$ ), which was smaller than the value for September to October ( $1.3 \times 10^{-3} \text{ mg Chl (mg C)}^{-1}$ ,  $N = 136$ ,  $p < 0.01$ ) (Fig. 6). Because  $\tau_{\min}$  decreased with increasing nutrient stress, there was stronger nutrient limitation during the former than the latter period. The fact that our  $\tau_{\min}$  was about half of the values in Behrenfeld et al. (2005), who reported that  $\tau_{\min}$  in the SPG L0 (the sea area where the climatological standard deviation of Chl was smaller than  $0.018 \text{ mg m}^{-3}$ ) was  $\sim 3.7 \times 10^{-3} \text{ mg Chl (mg C)}^{-1}$ , might have been due to the cSPG's being the most oligotrophic waters of the SPG L0. We also found that the MLD was much deeper ( $\sim 86.4$  to  $121.1 \text{ m}$ ) during September–October than during January–March ( $\sim 37.7$  to  $46.0 \text{ m}$ ) (Fig. 2b). The nature of these MLD variations suggested that more nutrients may have been upwelled from deeper layers during the period of September to October. That supposition is consistent with the  $\tau_{\min}$  value. According to the resource allocation theory of phytoplankton (Halsey & Jones, 2015), a lower nutrient supply would have resulted in lower nutrient allocation to light absorption (i.e., Chl) during January–March than during September–October.

As for the temperature effect, the  $\tau_{\max}$  value that gave the best fit was  $\sim 0.01 \text{ mg Chl (mg C)}^{-1}$  for September to October, and  $\sim 0.13 \text{ mg Chl (mg C)}^{-1}$  for January to March (Fig. 6). The sea-surface temperature (SST) was significantly lower during September–October ( $\sim 20.8$  to  $23.5 \text{ }^\circ\text{C}$ ) than during January–March ( $\sim 24.3$  to  $27.8 \text{ }^\circ\text{C}$ ) ( $p < 0.01$ ). The fact that our  $\tau_{\max}$  was consistent with the trend in Behrenfeld et al. (2005) showed that  $\tau_{\max}$  increases with increasing temperature. The implication is that there is more temperature limitation during the period from September to October than from January to March. However, the fact that the change of Chl was greater from September to October than that from January to March (Fig. 1b), which suggests that the influence of temperature limitation was less than the effects of nutrient limitation. This pattern might have been caused by the fact that the effects of temperature on photoacclimation are also a function of nutrient limitation, because the influence of temperature on phytoplankton physiology is nutrient dependent (Fernández-González et al., 2020). This dependence is consistent with the relationship between Chl and MLD ( $R^2 = 0.56$ ,  $N = 354$ ,  $p < 0.01$ ), which was higher than the  $R^2$  between Chl and SST ( $R^2 = 0.39$ ,  $N = 354$ ,  $p < 0.01$ ) during this period. These observations indicated that the impact of nutrient limitation on

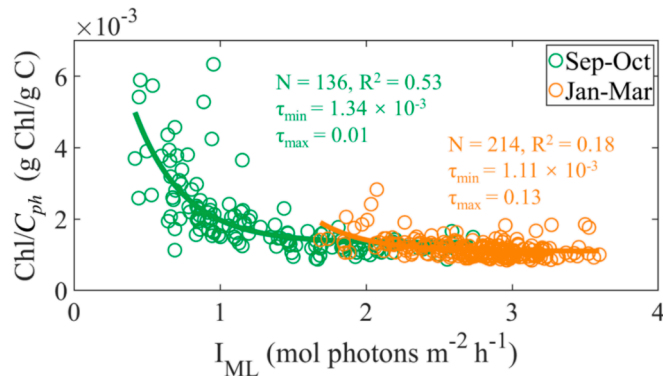


Fig. 6. The relationships between  $I_{ML}$  and  $\text{Chl}/C_{ph}$  in September–October time (green,  $N = 136$ ) and in January–March time (orange,  $N = 214$ ).

photoacclimation is greater than the impact of temperature.

We therefore accepted our hypothesis: the physiological status of phytoplankton from January to March was primarily limited by nutrients in the cSPG, thus phytoplankton were less responsive in terms of pigment regulation by photoacclimation during this period than during the period from September to October.

### 3.6. The phytoplankton's dynamics influenced by the alternation of co-regulation mechanisms

Our comprehensive analysis reveals that the dynamics of Chl in cSPG are governed by a complex interplay of multiple processes throughout the year (Fig. 7a). The co-regulated by these processes shapes the observed Chl- $\text{PAR}(0)$  “trapezoidal” patterns, reflecting the response of phytoplankton on changing environmental conditions. In our study, we focused more on the temporal variation in the intensity of controlling mechanisms. It's important to note that the phytoplankton primarily driven by photoacclimation, and the influence of zooplankton and nutrients on the phytoplankton remains in the whole year, while here we emphasized the strength switch of environmental factors. From April to August, cooling, dilution, and nutrient addition with intense deepening of the mixed layer promoted phytoplankton growth and accounted for the increase of Chl. In August, a continuous decrease of light availability and higher grazing by zooplankton led to a decrease of Chl. Though photoacclimation dominated during both periods, relatively high nutrient stress led to a lower rate of up-regulation of Chl from January to March than the rate of down-regulation of Chl from September to October. From November to December, Chl dynamics were controlled

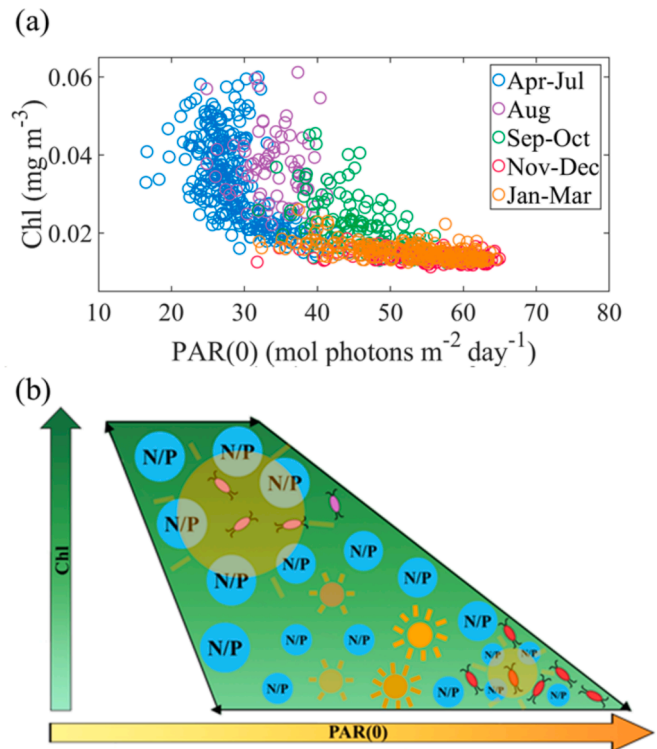
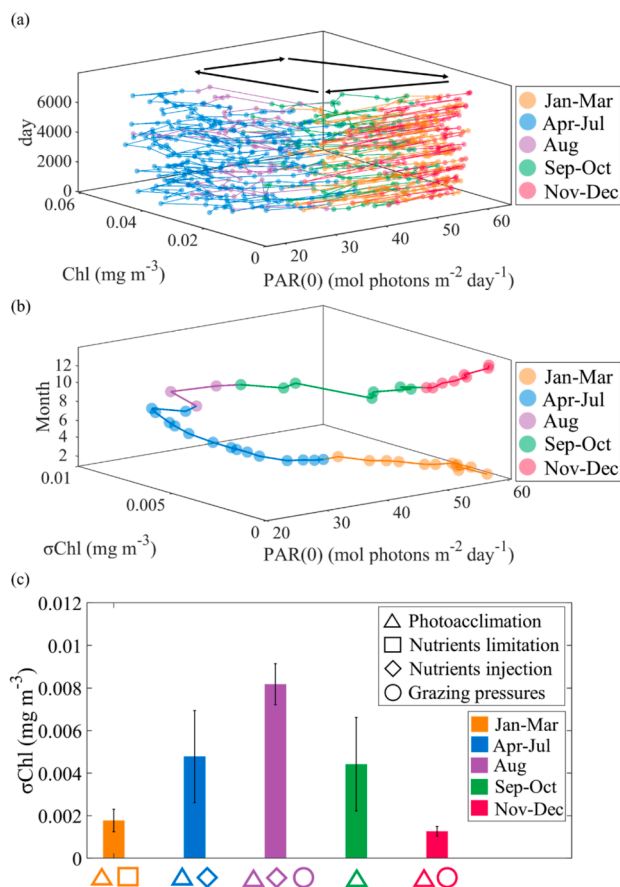


Fig. 7. Alternation of co-regulation mechanisms drives the “trapezoidal” pattern between Chl and  $\text{PAR}(0)$  in the cSPG. (a) The color represents different periods. Blue: from April to July ( $N = 274$ ,  $p < 0.01$ ); Purple: August ( $N = 75$ ,  $p = 0.11$ ); Green: from September to October ( $N = 138$ ,  $p < 0.01$ ); Red: from November to December ( $N = 147$ ,  $p < 0.01$ ); Orange: from January to March ( $N = 216$ ,  $p < 0.01$ ). (b) The conceptual scheme of dominated co-regulation mechanisms driving the “trapezoidal” relationship between Chl and  $\text{PAR}(0)$  in cSPG. Light color to deep color represents low-value and high-value of Chl (green) or  $\text{PAR}(0)$  (yellow).

not only by photoacclimation but also by grazing pressure from zooplankton. The result was the formation of a “trapezoidal” pattern between Chl and PAR(0) at the cSPG (Fig. 7b).

As discussed above, our concepts of steady state and non-steady state in this study focused more on an ecosystem than a culture system (Harris, 1988; Pahl-Wostl, 1995). Long-term observations by satellites over the cSPG revealed a “trapezoidal spiral structure” between Chl and PAR(0) (see Fig. 1b and Fig. 8a). The spiral structure reflected the changes of Chl at the same PAR(0) over a long period of time. From April to August, the lines appeared chaotic, and the intensity of the Chl dynamics indicated that a system characterized by such Chl dynamics was not easily returned to a previous state, indicated that the phytoplankton community is under a more dynamics scenario, approaching the non-steady state (Beninca et al., 2008; Naselli-Flores et al., 2003). In contrast, from November to December, the lines of Chl versus PAR(0) during different years were approximately parallel with each other. The implication was that the Chl was closer to recovering the previous state, suggested that the phytoplankton community is in the steady state (Rojo & Álvarez-Cobelas, 2003). The Chl dynamics from January to March and from September to October fell between the two aforementioned states: The phytoplankton state from September to October resembled the former, while the phytoplankton state from January to March resembled the latter. Overall, we could find on a long-time scale, the seasonal variation of Chl in the cSPG was a dynamic steady state regulated not solely by photoacclimation but rather a complex process. Specially, the steady state of phytoplankton community may be influenced by the alternation of co-regulation mechanisms.



**Fig. 8.** The combination of steady-state and non-steady state of phytoplankton in cSPG. (a) “Trapezoidal” spiral rise structure of Chl in cSPG on a long-time scale. (b) The climatological  $\sigma\text{Chl}$  from 2003 to 2020. (c) The averages of  $\sigma\text{Chl}$  dominated by each co-regulation mechanism. The color of markers/lines/bars and the symbol representation are the same as that in Fig. 7a.

Fig. 8b-8c show the climatological standard deviation of Chl ( $\sigma\text{Chl}$ ) from 2003 to 2020. Values of  $\sigma\text{Chl}$  were a minimum during November–December ( $1.3 \times 10^{-3} \text{ mg m}^{-3}$ ), and then it increased slowly from January to March ( $1.8 \times 10^{-3} \text{ mg m}^{-3}$ ).  $\sigma\text{Chl}$  increased sharply from April to July ( $4.8 \times 10^{-3} \text{ mg m}^{-3}$ ) and reached a maximum in August ( $8.2 \times 10^{-3} \text{ mg m}^{-3}$ ). Subsequently,  $\sigma\text{Chl}$  decreased from September to October ( $4.4 \times 10^{-3} \text{ mg m}^{-3}$ ). These results indicated that the balance between phytoplankton growth and zooplankton grazing temporarily stabilized the phytoplankton assemblage from November to December. During this period, the interactions between phytoplankton and zooplankton were the equilibrium force that strongly balanced the system (Gaedeke & Sommer, 1986). Equilibrium conditions were gradually destroyed by environmental disturbances and strength (i.e., both light and nutrient limitation) from January to March. The impact of the injection of nutrients was sufficient to disrupt the interactions between the phytoplankton and zooplankton from April to August (Harris, 1988). The dynamics of the phytoplankton assemblages was subsequently tempered by the reduction of nutrient inputs, and the phytoplankton were further influenced by light from September to October. Finally, the phytoplankton assemblages recover to steady-state from November to December.

Thus, based on the “observation window” of the climatological monthly temporal scale (Wu & Loucks, 1995), we therefore found that the “trapezoidal” spiral structure between Chl and PAR(0) in the cSPG reflects a complex and dynamic steady state of the phytoplankton assemblage (Fig. 8a). This study demonstrates that steady-states of phytoplankton assemblages indeed exist within this ecosystem, with equilibrium forces primarily driven by interactions among phytoplankton and zooplankton in the cSPG (Sommer et al., 1993). The results of this study also support the theory of non-steady state dynamics that emphasizes the nested and interacting processes influencing the ecosystem on different temporal scales (Allen & Starr, 1982). Overall, a long-term “trapezoidal” relationship between Chl and PAR(0) implied that phytoplankton’s steady state may be influenced by the alternation of co-regulation mechanisms, but it will reach the steady state with temporally varying environments in cSPG throughout the year.

### 3.7. Other processes and other subtropical gyres

Results from MLR analysis indicated that photoacclimation, nutrients, and grazing pressures by zooplankton could explain  $\sim 84\%$  of the Chl variance ( $R^2 = 0.84$ ,  $p < 0$ ), while the remaining ( $\sim 16\%$ ) Chl variance was contributed by other processes. It is worth noting that different phytoplankton ecotypes exhibit varying rates of photoacclimation and photosynthesis in response to changing light conditions (Casey et al., 2022). Additionally, these ecotypes often display preferences for specific seasonal conditions (Flombaum et al., 2020) that potentially contribute to the observed “trapezoidal” pattern between Chl and PAR(0) in the cSPG. Another process that may have contributed to the phytoplankton dynamics was the deposition of aerosols from the atmosphere into the ocean. Aerosols can carry essential nutrients, such as iron, that promote phytoplankton growth (Duce et al., 1991; Duce, 1986). Previous studies have indicated precipitation rates are lower during local summer compared to local winter in the SPG (Duce et al., 1991). The implication is that more micronutrients might be transferred from the atmosphere to the ocean in winter. This increased input of micronutrients from deposition could accelerate the increase of Chl during the winter months. Another process that may have led to higher rates of down-regulation of Chl from September to October than rates of up-regulation of Chl from January to March might have been more violent mixing dynamics during the former period. Brunet (2003) have demonstrated that photoacclimation can be a metric used to estimate vertical water movements based on the positive relationship between mixing and the rate of change of photoacclimation parameters. In our study, there was a greater change of the MLD during September–October ( $\sim 34.7 \text{ m}$ ) than during January–March ( $\sim 8.3 \text{ m}$ ) (Fig. 2b). The more

intense dynamics of the MLD may have led to a more rapid response of phytoplankton to variations in the light field from September to October compared to the period of January to March (Fig. 1b).

It appears that the “trapezoidal” relationship between Chl and PAR(0) also exists at the center of other subtropical gyres: the centers of the North Atlantic Gyre (cNATL, 25° – 30° N and 55° – 60° W), the South Atlantic Gyre (cSATL, 15° – 20° S and 25° – 30° W), and the Indian Ocean Gyre (cIO, 25° – 30° S and 75° – 80° E) (Fig. 9a-e). These results indicate that the “trapezoidal” relationship between Chl and PAR(0) may be a general pattern that reflects some degree of environmental similarity. An obvious “outlier” is the center of the North Pacific Gyre (cNPG, 12° – 17° N and 160° – 165° E) (Fig. 9f), where processes in addition to those we have discussed (e.g., nitrogen fixation (Friedrich et al., 2021), Ekman convergence (Chow et al., 2019), dust deposition (Tan et al., 2016)) might also play important roles in the Chl dynamics. A detailed description of Chl variations in the cNPG is beyond the scope of this study, but examination of the relationship between Chl and PAR(0) in five subtropical gyres has demonstrated that the relationship in the cNPG is unlike the relationships in the other four marine areas (Hardman-Mountford et al., 2008; Vichi et al., 2011). A challenge for future studies is to determine why there are large regional differences between some ocean gyres. Moreover, we recommend incorporating more techniques into future analyses, such as the use of Biogeochemical Argo (BGC-Argo) floats. These instruments can capture high-resolution water profiles, thereby providing further evidence to support the Chl-driven mechanisms under investigation. Answers to such questions will help us to obtain a more comprehensive understanding of the mechanisms that drive the temporal dynamics of Chl and refine our understanding of phytoplankton responses to ongoing climate changes.

#### 4. Conclusions

Our study suggested that an alternation of co-regulation mechanisms drives the “trapezoidal” relationship between Chl and PAR(0) at the cSPG. The implication is that nested and interactive processes influence the same ecosystem at different temporal scales. Although the dynamics of phytoplankton Chl involves complex processes, our results suggest how an ecological model and a forecasting model might be optimized. Most previous forecasting models that predict how global warming will affect phytoplankton in the future have focused more on one dominant effect (e.g., SST, light, or MLD dynamics) (Behrenfeld et al., 2006, 2016; Boyce et al., 2010; Toseland et al., 2013). Although these studies have considered the effects of multiple factors on phytoplankton, they have generally modeled the effect (positive or negative) of one factor on phytoplankton as if there were no interaction between factors, because each subsystem was assumed separately rather than collectively (Boyce et al., 2010; Laws et al., 2000; Plattner, 2005). While photoacclimation, nutrient limitation, temperature, and other processes have been considered in some ecological models, the temporal alternation and interplay of these processes have been neglected (Sathyendranath et al., 2020; Siemer et al., 2021; Westberry et al., 2008). Because the contribution of each mechanism on Chl variability differed between periods of the year, disregarding this pattern might lead to significant errors in model-estimated Chl. Going forward, we ought to optimize ecological models and forecasting models by focusing more on the different impacts of these processes on primary producers at different times of the year.

However, it’s necessary to emphasize the suitability of steady state models and the need to choose the appropriate assumption based on the specific research goals. It’s worth noting that global-scale studies might

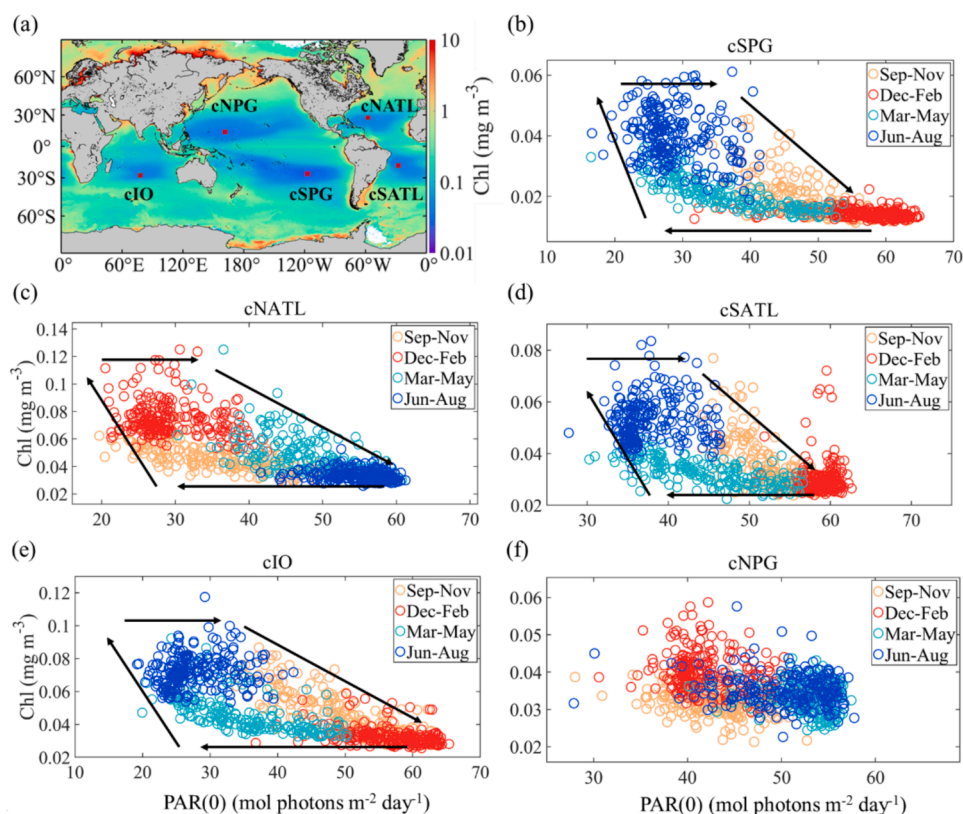


**Fig. 9.** The relationships between Chl and PAR(0) at the centers of classic subtropical gyres. (a) The red points show the centers of five subtropical gyres. The background color is the average climatological Chl derived from MODIS Aqua downloaded from NASA OBPG, which have a spatial resolution of 9 km and a temporal resolution of 8-day from 2002 to 2020. (b-e) The “trapezoidal” relationships between Chl and PAR(0) at cSPG, cNATL, cSATL and cIO, respectively. (f) The “non-trapezoid” relationship between Chl and PAR(0) at cNPG. (b-f) Colors are denoted by seasons. Orange circles: September to November; Red circles: December to February; Green circles: March to May; Blue circles: June to August.

be more suitable for employing a steady-state assumption, primarily due to their substantial computational resource requirements. The utilization of a steady-state assumption serves to optimize computational resources and simultaneously mitigating the risk of overfitting. While, when focused on the spatiotemporal variations of specific sea area and a desire to meet heightened precision requirements, both steady-state and non-steady-state assumptions are recommended.

The results of this work remind us that in future ecological studies, more attention should be paid on the alternation of steady state and non-steady-state conditions rather than assuming steady state conditions throughout the year. In this way we will obtain a more comprehensive understanding about how phytoplankton respond to contemporary climate variability.

### CRedit authorship contribution statement

**Dongmei Lian:** Writing – original draft, Investigation, Formal analysis. **Xin Liu:** Writing – review & editing, Project administration, Formal analysis, Conceptualization. **Edward A. Laws:** Writing – review & editing, Formal analysis. **Tongtong Liu:** Investigation. **Jingxiao Wang:** Investigation. **Shaoling Shang:** Writing – review & editing, Formal analysis. **Zhongping Lee:** Writing – review & editing, Project administration, Formal analysis, Conceptualization.

### Declaration of competing interest

The authors declare that they have no known competing financial interests or personal relationships that could have appeared to influence the work reported in this paper.

### Data availability

Data will be made available on request.

### Acknowledgements

Financial support by the National Natural Science Foundation of China (#41890803, #41830102 #41941008, #42250710150) is greatly appreciated. The authors would like to thank NASA for the distribution of MODIS ocean color products and two anonymous reviewers for constructive comments and suggestions.

### References

- Allen, T., Starr, T., 1982. Hierarchy: Perspectives for Ecological Complexity. *SERBIULA (Sistema Librum 2.0)*.
- Almén, A.-K., Tamelander, T., 2020. Temperature-related timing of the spring bloom and match between phytoplankton and zooplankton. *Mar. Biol. Res.* 16, 674–682.
- Austin, R.W., Petzold, T.J., 1981. The Determination of the Diffuse Attenuation Coefficient of Sea Water Using the Coastal Zone Color Scanner. Springer, US.
- Behrenfeld, M.J., 2010. Abandoning Sverdrup's Critical Depth Hypothesis on phytoplankton blooms. *Ecology* 91, 977–989.
- Behrenfeld, M.J., Marañón, E., Siegel, D.A., Hooker, S.B., 2002. Photoacclimation and nutrient-based model of light-saturated photosynthesis for quantifying oceanic primary production. *Mar. Ecol. Prog. Ser.* 228, 103–117.
- Behrenfeld, M.J., Boss, E., Siegel, D.A., Shea, D.M., 2005. Carbon-based ocean productivity and phytoplankton physiology from space. *Global Biogeochem. Cycles* 19.
- Behrenfeld, M.J., O'Malley, R.T., Siegel, D.A., McClain, C.R., Sarmiento, J.L., Feldman, G.C., Milligan, A.J., Falkowski, P.G., Letelier, R.M., Boss, E.S., 2006. Climate-driven trends in contemporary ocean productivity. *Nature* 444, 752–755.
- Behrenfeld, M.J., O'Malley, R.T., Boss, E.S., Westberry, T.K., Graff, J.R., Halsey, K.H., Milligan, A.J., Siegel, D.A., Brown, M.B., 2016. Reevaluating ocean warming impacts on global phytoplankton. *Nat. Clim. Chang.* 6, 323–330.
- Beninca, E., Huisman, J., Heerkloss, R., Johnk, K.D., Branco, P., Van Nes, E.H., Scheffer, M., Ellner, S.P., 2008. Chaos in a long-term experiment with a plankton community. *Nature* 451, 822–825.
- Boss, E., Behrenfeld, M., 2010. In situ evaluation of the initiation of the North Atlantic phytoplankton bloom. *Geophys. Res. Lett.* 37.
- Boyce, D.G., Lewis, M.R., Worm, B., 2010. Global phytoplankton decline over the past century. *Nature* 466, 591–596.
- Boyce, D.G., Petrie, B., Frank, K.T., Worm, B., Leggett, W.C., 2017. Environmental structuring of marine plankton phenology. *Nat. Ecol. Evol.* 1, 1484–1494.
- Brunet, C., 2003. Measured photophysiological parameters used as tools to estimate vertical water movements in the coastal Mediterranean. *J. Plankton Res.* 25, 1413–1425.
- Cara, W., Victoria, J., Coles, 2005. Global climatological relationships between satellite biological and physical observations and upper ocean properties. *J. Geophys. Res. Oceans*.
- Casey, J.R., Boiteau, R.M., Engqvist, M.K., Finkel, Z.V., Li, G., Liefer, J., Müller, C.L., Muñoz, N., Follows, M.J., 2022. Basin-scale biogeography of marine phytoplankton reflects cellular-scale optimization of metabolism and physiology. *Sci. Adv.* 8, eabl4930.
- Chow, C.H., Cheah, W., Tai, J.-H., Liu, S.-F., 2019. Anomalous wind triggered the largest phytoplankton bloom in the oligotrophic North Pacific Subtropical Gyre. *Sci. Rep.* 9.
- Claustre, H., Sciandra, A., Vulot, D., 2008. Introduction to the special section bio-optical and biogeochemical conditions in the South East Pacific in late 2004: the BIOSOPE program. *Biogeosciences* 5, 679–691.
- Cloern, J.E., Grenz, C., Vidregar-Lucas, L., 1995. An empirical model of the phytoplankton chlorophyll : carbon ratio-the conversion factor between productivity and growth rate. *Limnol. Oceanogr.* 40, 1313–1321.
- Cohen, J., Cohen, P., West, S.G., Aiken, L.S., 2013. *Applied multiple regression/correlation analysis for the behavioral sciences*.
- Dandonneau, Y., Vega, A., Loisel, H., Penhoat, Y.D., Menkes, C., 2003. Oceanic Rossby Waves Acting As a "Hay Rake" for ecosystem floating by-products. *Science* 302, 1548–1551.
- Doney, S.C., Glover, D.M., McCue, S.J., Fuentes, M., 2003. Mesoscale variability of Sea-viewing Wide Field-of-view Sensor (SeaWiFS) satellite ocean color: Global patterns and spatial scales. *J. Geophys. Res. Oceans* 108.
- Duce, R.A., 1986. The impact of atmospheric nitrogen, phosphorus, and iron species on marine biological productivity. In: *The Role of Air-Sea Exchange in Geochemical Cycling*. Springer, pp. 497–529.
- Duce, R., Liss, P., Merrill, J., Atlas, E., Buat-Menard, P., Hicks, B., Miller, J., Prospero, J., Arimoto, R., Church, T., 1991. The atmospheric input of trace species to the world ocean. *Global Biogeochem. Cycles* 5, 193–259.
- Dufois, F., Hardman-Mountford, N.J., Greenwood, J., Richardson, A.J., Matear, R.J., 2016. Anticyclonic eddies are more productive than cyclonic eddies in subtropical gyres because of winter mixing. *Sci. Adv.* 2.
- Edwards, K.F., Thomas, M.K., Klausmeier, C.A., Litchman, E., 2012. Allometric scaling and taxonomic variation in nutrient utilization traits and maximum growth rate of phytoplankton. *Limnol. Oceanogr.* 57, 554–566.
- Fernández-González, C., Pérez-Lorenzo, M., Pratt, N., Moore, C.M., Bibby, T.S., Marañón, E., 2020. Effects of temperature and nutrient supply on resource allocation, photosynthetic strategy, and metabolic rates of *Synechococcus* sp. *J. Phycol.* 56, 818–829.
- Flombaum, P., Wang, W.-L., Primeau, F.W., Martiny, A.C., 2020. Global picophytoplankton niche partitioning predicts overall positive response to ocean warming. *Nat. Geosci.* 13, 116–120.
- Fox, J., Kramer, S.J., Graff, J.R., Behrenfeld, M.J., Boss, E., Tilstone, G., Halsey, K.H., 2022. An absorption-based approach to improved estimates of phytoplankton biomass and net primary production. *Limnology and Oceanography Letters* 7, 419–426.
- Friedrich, T., Powell, B.S., Stock, C.A., Hahn-Woernle, L., Dussan, R., Curchitser, E.N., 2021. Drivers of phytoplankton blooms in Hawaii: a regional model study. *J. Geophys. Res. Oceans* 126.
- Gaedeke, A., Sommer, U., 1986. The influence of the frequency of periodic disturbances on the maintenance of phytoplankton diversity. *Oecologia* 71, 25–28.
- Geider, R., 1987. Light and temperature dependence of the carbon to chlorophyll a ratio in microalgae and cyanobacteria: Implications for physiology and growth of phytoplankton. *New Phytol.* 106, 1–34.
- Geider, R.J., La Roche, J., 2002. Redfield revisited: variability of C [ratio] N [ratio] P in marine microalgae and its biochemical basis. *Eur. J. Phycol.* 37, 1–17.
- Gerald, B., 2018. A Brief Review of Independent, Dependent and One Sample t-test. *Int. J. Appl. Math. Theoret. Phys.* 4.
- Graff, J.R., Behrenfeld, M.J., 2018. Photoacclimation responses in subarctic Atlantic phytoplankton following a natural mixing-restratification event. *Front. Mar. Sci.* 5, 209.
- Halsey, K.H., Jones, B.M., 2015. Phytoplankton strategies for photosynthetic energy allocation. *Ann. Rev. Mar. Sci.* 7, 265–297.
- Hardman-Mountford, N.J., Hirata, T., Richardson, K.A., Aiken, J., 2008. An objective methodology for the classification of ecological pattern into biomes and provinces for the pelagic ocean. *Remote Sens. Environ.* 112, 3341–3352.
- Harris, G., 1988. Phytoplankton Ecology: Structure, Function and Fluctuation. *J. N. Am. Benthol. Soc.* 6.
- Hu, C., Lee, Z., Franz, B., 2012. Chlorophyll algorithms for oligotrophic oceans: A novel approach based on three-band reflectance difference. *J. Geophys. Res. Oceans* 117.
- Karl, D.M., Björkman, K.M., Church, M.J., Fujieki, L.A., Grabowski, E.M., Letelier, R.M., 2022. Temporal dynamics of total microbial biomass and particulate detritus at Station ALOHA. *Progress in Oceanography* 205, 102803.
- Kirk, J., 1983. *Light and Photosynthesis in Aquatic Ecosystems*. Cambridge University Press.
- Landry, M.R., Barber, R.T., Bidigare, R.R., Chai, F., Coale, K.H., Dam, H.G., Lewis, M.R., Lindley, S.T., McCarthy, J.J., Roman, M.R., 1997. Iron and grazing constraints on primary production in the central equatorial Pacific: An EqPac synthesis. *Limnol. Oceanogr.* 42, 405–418.
- Landry, M., Hassett, R., 1982. Estimating the grazing impact of marine microzooplankton. *Mar. Biol.* 67, 283–288.

- Landry, M., Kirshtein, J., Constantinou, J., 1995. A refined dilution technique for measuring the community grazing impact of microzooplankton, with experimental tests in the central equatorial Pacific. *Mar. Ecol. Prog. Ser.* 120, 53–63.
- Laws, E.A., Bannister, T.T., 1980. Nutrient- and light-limited growth of *Thalassiosira fluviatilis* in continuous culture, with implications for phytoplankton growth in the ocean. *Limnol. Oceanogr.* 25, 457–473.
- Laws, E.A., Falkowski, P.G., Smith, W.O., Ducklow, H., McCarthy, J.J., 2000. Temperature effects on export production in the open ocean. *Global Biogeochem. Cycles* 14, 1231–1246.
- Lynam, C.P., Llope, M., Mollmann, C., Helouet, P., Bayliss-Brown, G.A., Stenseth, N.C., 2017. Interaction between top-down and bottom-up control in marine food webs. *Proc. Natl. Acad. Sci.* 114, 1952–1957.
- Macintyre, H.L., Kana, T.M., Anning, T., Geider, R.J., 2002. Photoacclimation of Photosynthesis Irradiance Response Curves and Photosynthetic Pigments in Microalgae and Cyanobacteria 1. *J. Phycol.* 38.
- Maritorena, S., Siegel, D.A., Peterson, A.R., 2002. Optimization of a semi-analytical ocean color model for global-scale applications. *Appl. Opt.* 41, 2705–2714.
- McClain, C., 2009. A Decade of Satellite Ocean Color Observations. *Ann. Rev. Mar. Sci.* 1, 19–42.
- McClain, C.R., Signorini, S.R., Christian, J.R., 2004. Subtropical gyre variability observed by ocean-color satellites. *Deep Sea Res. Part II* 51, 281–301.
- Middleton, N., Kang, U., 2017. Sand and dust storms: Impact mitigation. *Sustainability* 9, 1053.
- Moeller, H.V., Laufkotter, C., Sweeney, E.M., Johnson, M.D., 2019. Light-dependent grazing can drive formation and deepening of deep chlorophyll maxima. *Nat. Commun.* 10, 1978.
- Morel, A., Huot, Y., Gentili, B., Werdell, P.J., Hooker, S.B., Franz, B.A., 2007. Examining the consistency of products derived from various ocean color sensors in open ocean (Case 1) waters in the perspective of a multi-sensor approach. *Remote Sens. Environ.* 111, 69–88.
- Naselli-Flores, L., Padisák, J., Dokulil, M.T., Chorus, I., 2003. Equilibrium/steady-state concept in phytoplankton ecology. *Phytoplankton and Equilibrium Concept: The Ecology of Steady-State Assemblages*. Springer, pp. 395–403.
- O'Brien, T.D., Wiebe, P.H., Falkenhaus, T., 2013. *ICES zooplankton status report 2010/2011: ICES Cooperative Research Reports (CRR)*.
- Pahl-Wostl, C., 1995. The dynamic nature of ecosystems: chaos and order entwined. *Plattner, G.-K.*, 2005. Decoupling marine export production from new production. *Geophys. Res. Lett.* 32.
- Qi, L., Lee, Z., Hu, C., Wang, M., 2017. Requirement of minimal signal-to-noise ratios of ocean color sensors and uncertainties of ocean color products. *J. Geophys. Res. Oceans* 122, 2595–2611.
- Rojo, C., Álvarez-Cobelas, M., 2003. Are there steady-state phytoplankton assemblages in the field? , *Phytoplankton and Equilibrium Concept: The Ecology of Steady-State Assemblages* (pp. 3-12): Springer.
- Sakshaug, E., Andresen, K., Kiefer, D.A., 1989. A steady state description of growth and light absorption in the marine planktonic diatom *Skeletonema costatum*. *Limnol. Oceanogr.* 34.
- Sathyendranath, S., Platt, T., Kovač, Ž., Dingle, J., Jackson, T., Brewin, R.J., Franks, P., Marañón, E., Kulk, G., Bouman, H.A., 2020. Reconciling models of primary production and photoacclimation. *Appl. Opt.* 59, C100–C114.
- Serra-Pompei, C., Hickman, A., Britten, G.L., Dutkiewicz, S., 2023. Assessing the potential of backscattering as a proxy for phytoplankton carbon biomass. *Global Biogeochemical Cycles*, e2022GB007556.
- Siemer, J.P., Machín, F., González-Vega, A., Arrieta, J.M., Gutiérrez-Guerra, M.A., Pérez-Hernández, M.D., Vélez-Belchí, P., Hernández-Guerra, A., Fraile-Nuez, E., 2021. Recent trends in SST, Chl-a, productivity and wind stress in upwelling and open ocean areas in the upper eastern North Atlantic Subtropical Gyre. *J. Geophys. Res. Oceans* 126.
- Signorini, S.R., Franz, B.A., McClain, C.R., 2015. Chlorophyll variability in the oligotrophic gyres: mechanisms, seasonality and trends. *Front. Mar. Sci.* 2.
- Sommer, U., 1988. Phytoplankton succession in microcosm experiments under simultaneous grazing pressure and resource limitation. *Limnol. Oceanogr.* 33, 1037–1054.
- Sommer, U., Padisák, J., Reynolds, C.S., Juhász-Nagy, P., 1993. Hutchinson's heritage: the diversity-disturbance relationship in phytoplankton. *Hydrobiologia* 249, 1–7.
- Talley, L.D., 1999. Some aspects of ocean heat transport by the shallow, intermediate and deep overturning circulations. *Geophys. Monograph-American Geophysical Union* 112, 1–22.
- Tan, S., Li, J., Gao, H., Wang, H., Che, H., Chen, B., 2016. Satellite-observed transport of dust to the East China Sea and the North Pacific Subtropical Gyre: Contribution of dust to the increase in chlorophyll during spring 2010. *Atmos.* 7, 152.
- Thingstad, T.F., Rassoulzadegan, F., 1995. Nutrient limitations, microbial food webs and 'biological C-pumps': suggested interactions in a P-limited Mediterranean. *Mar. Ecol. Prog. Ser.* 299–306.
- Toseland, A., Daines, S.J., Clark, J.R., Kirkham, A., Strauss, J., Uhlig, C., Lenton, T.M., Valentin, K., Pearson, G.A., Moulton, V., Mock, T., 2013. The impact of temperature on marine phytoplankton resource allocation and metabolism. *Nat. Clim. Chang.* 3, 979–984.
- Vichi, M., Allen, J.I., Masina, S., Hardman-Mountford, N.J., 2011. The emergence of ocean biogeochemical provinces: A quantitative assessment and a diagnostic for model evaluation. *Global Biogeochem. Cycles* 25 n/a-n/a.
- Werdell, P.J., Bailey, S.W., 2005. An improved in-situ bio-optical data set for ocean color algorithm development and satellite data product validation. *Remote Sens. Environ.* 98, 122–140.
- Westberry, T., Behrenfeld, M.J., Siegel, D.A., Boss, E., 2008. Carbon-based primary productivity modeling with vertically resolved photoacclimation. *Global Biogeochem. Cycles* 22, n/a-n/a.
- Wilson, C., Coles, V.J., 2005. Global climatological relationships between satellite biological and physical observations and upper ocean properties. *J. Geophys. Res. Oceans* 110.
- Wu, J., Loucks, O.L., 1995. From balance of nature to hierarchical patch dynamics: a paradigm shift in ecology. *Q. Rev. Biol.* 70, 439–466.
- Xing, X., Boss, E., Chen, S., Chai, F., 2021. Seasonal and daily-scale photoacclimation modulating the phytoplankton chlorophyll-carbon coupling relationship in the mid-latitude Northwest Pacific. *J. Geophys. Res.: Oceans* 126.
- Xiu, P., Chai, F., 2021. Impact of Atmospheric Deposition on Carbon Export to the Deep Ocean in the Subtropical Northwest Pacific. *Geophys. Res. Lett.* 48.
- Zehr, J.P., Capone, D.G., 2020. Changing perspectives in marine nitrogen fixation. *Science* 368.
- Zhang, Y., Mahowald, N., Scanza, R.A., Journet, E., Desboeufs, K., Albani, S., Kok, J.F., Zhuang, G., Chen, Y., Cohen, D.D., Paytan, A., Patey, M.D., Achterberg, E.P., Engelbrecht, J.P., Fomba, K.W., 2015. Modeling the global emission, transport and deposition of trace elements associated with mineral dust. *Biogeosciences* 12, 5771–5792.